Molecular Crystals and Liquid Crystals
Publication details, including instructions for authors and subscription information:
http://www.tandfonline.com/loi/gmcl16

Spatial Distribution of the Distribution of the Electroluminescence and the Recombination Process in Tetracene Single Crystals

J. Gliński [a] , J. Godlewski [a] & J. Kalinowski [a]
[a] Institute of Physics, Technical University of Gdańsk, 80-952, Gdańsk, Poland
Version of record first published: 28 Mar 2007.

To cite this article: J. Gliński , J. Godlewski & J. Kalinowski (1978): Spatial Distribution of the Distribution of the Electroluminescence and the Recombination Process in Tetracene Single Crystals, Molecular Crystals and Liquid Crystals, 48:1-2, 1-25

To link to this article: http://dx.doi.org/10.1080/00268947808083749

Mol. Cryst. Liq. Cryst., 1978, Vol. 48, pp. 1–26

Printed in Holland

Spatial Distribution of the Electroluminescence and the Recombination Process in Tetracene Single Crystals†

J. GLIŃSKI, J. GODLEWSKI, and J. KALINOWSKI

Institute of Physics, Technical University of Gdańsk, 80-952 Gdańsk, Poland

(*Received February 28, 1978; in final form May 18, 1978*)

The spectral dependence of the recombination electroluminescence (REL) to photoluminescence (PH) ratio has been used as an experimental probe for studying the physical characteristics of the recombination in tetracene.

A method is developed for determination of REL spatial distribution. In all crystals studied, under conditions where two injecting contacts are used, the light emission is concentrated in front of the electrodes. At a sufficiently high voltage applied, a splitting up of the light emission zone in two layers is found in front of the anode.

These experimental results can be explained qualitatively assuming appropriate gradients of charge densities, charge-quenching of the delayed component of the REL and charge density-dependence of the probability of a recombining electron-hole pair to yield a singlet exciton.

1 INTRODUCTION

The recombination electroluminescence (REL) is the most striking feature of double injection, and its spatial distribution in a crystal has to be in correspondence to volume-controlled currents (VCC). An extensive treatment of steady-state VCC is given in Refs. 1 to 5.

Under VCC flow the positive and negative space charges overlap leading to recombination transitions which are followed by both radiative and non-radiative decay. Thus, one would expect the space-charge overlap to be, in general, responsible for the spatial distribution of REL.

† Research supported in part by the Polish Academy of Sciences under program MR.I.9.

If the electron-hole recombination rate constant c in a trap-free crystal is sufficiently large, double injection from two ohmic contacts will produce two SCL currents meeting and annihilating each other within a luminous layer somewhere in the crystal. The location of this luminous zone is then determined by the ratio of electron and hole mobilities and its width by the relation between a combination of these mobilities and the so called recombination mobility $\mu_0 = \varepsilon_0 \varepsilon c/2e$ (see e.g. Ref. 1). Trapping effects under double injection can change this picture entirely.

A large number of deep traps causes the average thermal release time (τ_{REL}) to be much longer than the recombination time (τ_{REC}) and both of them to be much longer than the trapping time (τ_t).

Assuming that holes and electrons obey the same inequalities a splitting up of the recombination zone in two regions in front of the electrodes should appear. This, in contrast to impure anthracene,[1,6] can be the case with tetracene[7] and ultra-high purity anthracene crystals[8] as they contain the concentration of deep electron traps comparable to that for holes.

One of the two emitting regions may be separated from a suitable electrode when the above mentioned inequality is not valid either for holes or for electrons.

The radiative processes in the crystal involve not only single exciton pathways but also certain biexitonic mechanisms. The thermally induced singlet exciton (S) fission into two triplets and triplet–triplet annihilation leading to a singlet exciton have been found to play an important role in tetracene REL.[9,10] The thermally induced fission pathway reducing the efficiency of the prompt electroluminescence (PREL) is the inverse of the annihilation mechanism which is responsible for the delayed electroluminescence (DREL). The destruction of excitons by charge carriers is reflected in a drop of REL. Due to the long lifetime, triplet excitons (T) are quenched much more efficiently than singlets. Thus, the intensity ratio DREL/PREL is a function of charge concentration and the spatial distribution of REL constitutes a superposition of two different distributions corresponding to PREL and DREL.

As a result, more than two emitting regions in the crystal might be expected. Consequently, the occurrence of a layer structure in the spatial distribution of REL leads to several conclusions as to the relative concentration of traps and their distribution in energy on the one hand and to some informations on the recombination process in the crystal, on the other hand.

We have recently outlined[11] how the REL spatial distribution in thin organic crystals can be determined, and presented the preliminary results obtained with two tetracene single crystals.

We now wish to report the results of more detailed experimental studies of the REL spatial distribution in tetracene crystals, present an extended

description of the method and a theoretical consideration, which accounts for the observed features and gives good agreement with the data.

2 DESCRIPTION OF THE METHOD

The self-absorption of part of the fluorescence emission is utilized in a proposed method for determining of a spatial distribution of REL.

The principle of the method is the following: the unknown spatial distribution of REL ($\varphi(x)$) in a crystal is associated with the experimentally observed REL ($\Phi_{REL}(l_0)$) by the expression

$$\Phi_{REL}(l_0) = A(l_0) \int_0^d \varphi(x) \exp\left(-\frac{x}{l_0}\right) dx, \tag{1}$$

where $\exp(-x/l_0)$ stands for the photon escape probability when the emission takes place at a distance x from the crystal surface observed. $l_0 = \varepsilon_0^{-1}$ to be called observation depth, is the reciprocal of the absorption coefficient ε_0 of the fluorescent light. The integral runs along the whole thickness of the crystal d.

The quantity $A(l_0)$ is independent of x and contain such parameters as the quantum yield of fluorescence, the function which maps out the emission spectrum of the crystal singlets, and some apparatus factors associated with conditions of emission measurements. In principle, $\varphi(x)$ could be obtained from (1), however since reabsorption and spectral characteristics of various apparatus elements influence the fluorescence spectrum measured, it is very difficult to estimate the quantity $A(l_0)$.

Therefore, we relate $\Phi_{REL}(l_0)$ to the photoluminescence (PH) measured under the same conditions,

$$\Phi_{PH}(l_0) = A(l_0) \int_0^d S(x) \exp\left(-\frac{x}{l_0}\right) dx, \tag{2}$$

by the ratio $\Phi_{REL}(l_0)/\Phi_{PH} = F(l_0)$ which as a function of l_0, by a constant factor associated with intensity of excitation (I_0) and voltage (U) applied to the crystal in the case of REL, illustrates a difference between $\varphi(x)$ and the exciton distribution $S(x)$ obtained with the exciting light of wavelength λ_a (the penetration depth l_a of the exciting light is given by the reciprocal of its absorption coefficient ε_a).

The condition that permit the experimental ratio $F(l_0)$ to be used for determination of $\varphi(x)$ is to know function $S(x)$ which, in general, is modified by reabsorption. This modification is, however, negligible for the crystals with a low quantum yield of fluorescence.

The fluorescence quantum yield of tetracene crystals at room temperature is very low (~ 0.002)[12,13] and one can safely assume $S(x) = S(0)\exp(-x/l_a)$.† Then, (1) and (2) lead to an integral equation

$$\int_0^d \varphi(x)\exp\left(-\frac{x}{l_0}\right) = f(l_0), \tag{3}$$

where

$$f(l_0) = F(l_0)S(0)\frac{l_0 l_a}{l_0 + l_a}\left[1 - \exp\left(-\frac{l_0 + l_a}{l_0 l_a}d\right)\right] \tag{4}$$

with $S(0) = I_0\tau_S/l_a$ (τ_S is the lifetime of singlet excitons).

Equation (3) can be solved by the method of statistical regularization.[14] This method consists in introducing an a priori information about the unknown function $\varphi(x)$. In our case it is an information about the smoothness and nonnegativity of the solution. The assumption on the smoothness of the unknown function is done by imposing the probabilistic restrictions on the value of a certain functional computed using the values of the function at support points.

Using the apparatus of mathematical statistics known as the Bayesian strategy (see e.g. Ref. 15), we obtain a "regularized" solution and its rms errors. The details of this procedure are given in Appendix A and testing of the method in Appendix B.

3 EXPERIMENTAL PROCEDURE AND RESULTS

In order to record REL and PH under identical observation conditions, the special experimental arrangement has been completed (Figure 1). It gives an independent possibility to measure REL or PH with the same optical and detection systems.

Vapour grown tetracene single crystals‡ with well-developed (*ab*) plane and typical thickness between 90 μm and 250 μm were supplied with electron (Na/K) and hole (Au or Hg) injecting contacts.

The emission leaving the crystal passed a lens (L_2), a polarizer (P) oriented parallel to the *b* axis of the crystal, a monochromator (Zeiss model SPM-2)

† $S(x)$ can also be influenced by nonradiative processes as for example excitonic diffusion. Since, however, the singlet exciton diffusion length in tetracene crystals at room temperature is 120 Å[24] the diffusion-induced modification of $S(x)$ is to be negligible

Due to the low singlet–triplet transition moment other nonradiative transitions in tetracene crystals seem not to play any significant role for the shape of $S(x)$.

These predictions are confirmed by the STREG-method determined $S(x)$ generated with the light of wavelength $\lambda_u = 366$ nm (see Appendix B).

‡ The crystals were kindly given to us by Prof. H. Baessler.

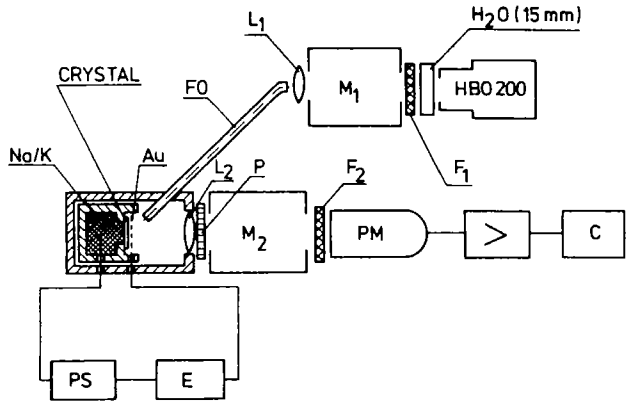

FIGURE 1 Schematic drawing of the experimental arrangement permitting the spectral measurements of REL or PH to be performed with the same optical and detection systems. The cell is made of cross-linked polyethylene and placed in the black-coated brass housing. The crystal is attached with paraffin wax; the observed emission, in both cases, is formed into a beam with the lens (L_2), transmitted through a polarizer (P), a monochromator M_2 and the colour filter F_2 and detected by the photomultiplier PM; PS power supply for double injection into the crystal; E electrometer.

The measurements of fluorescence were made with PS being switched off and both electrodes grounded. Additional informations concerning this Figure are given in the text.

with the output colour filter F_2 (Schott GG-14) to an EMI 6256 S photomultiplier. The photomultiplier signals were amplified and counted by a pulse counter (C).

The tetracene fluorescence was excited at 436 nm by a high-pressure mercury lamp (Zeiss HBO-200) followed by a heat filter, a colour filter F_1 (Corning 5-58), a monochromator (Zeiss model SPM-2), a lens L_1, and conducted through a light guide to the crystal surface observed.

Both REL and PH were observed through a semitransparent gold layer used in the case of REL as the electrode injecting holes.

The double injected currents were measured using the normal apparatus and technique. Before undertaking the above described analysis for obtaining spatial REL distribution, it is necessary to measure the ratio of REL to PH intensity as a function of emission wavelength λ_0. Figure 2 shows the measured change of the ratio Φ_{REL}/Φ_{PH} with increasing observation depth (l_0).

The values of l_0 are based on the tetracene absorption spectrum from Ref 16 (see also Ref. 17) in the short emission wavelength range and from Ref 18 in the long-wavelength region.

According to Ref. 10 the difference between REL and PH spectra in the long-wavelength region ($l_0 \gtrsim 10^3$ μm) is due to a higher efficiency of the trapped exciton production in the case of the REL as compared to the PH.

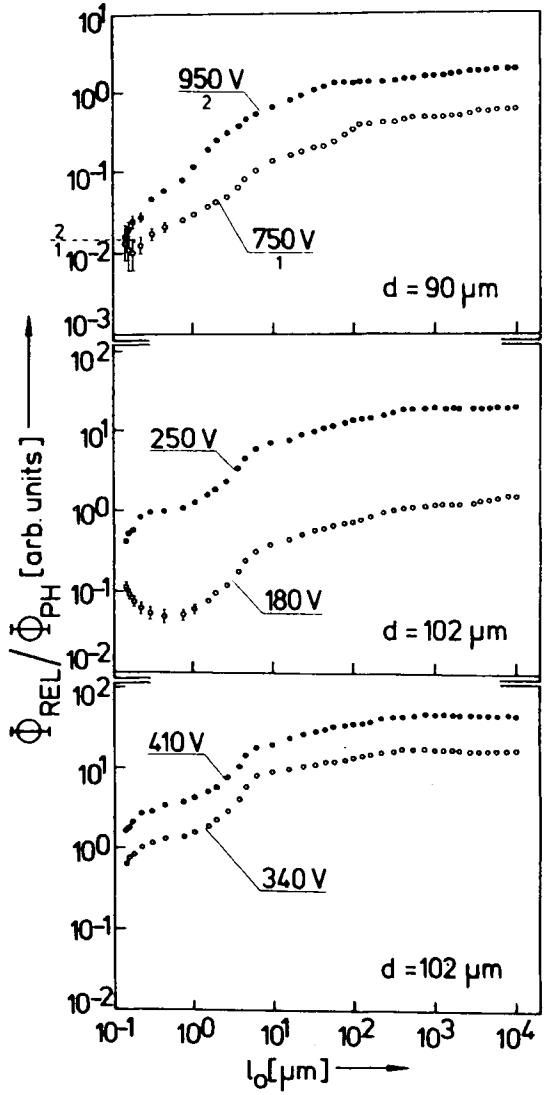

FIGURE 2(a) Experimental dependence of the recombination electroluminescence (Φ_{REL}) to photoluminescence (Φ_{PH}) ratio as a function of observation depth (l_0) for 5 different tetracene crystals with various voltages applied to the crystals when the REL was under measurements.

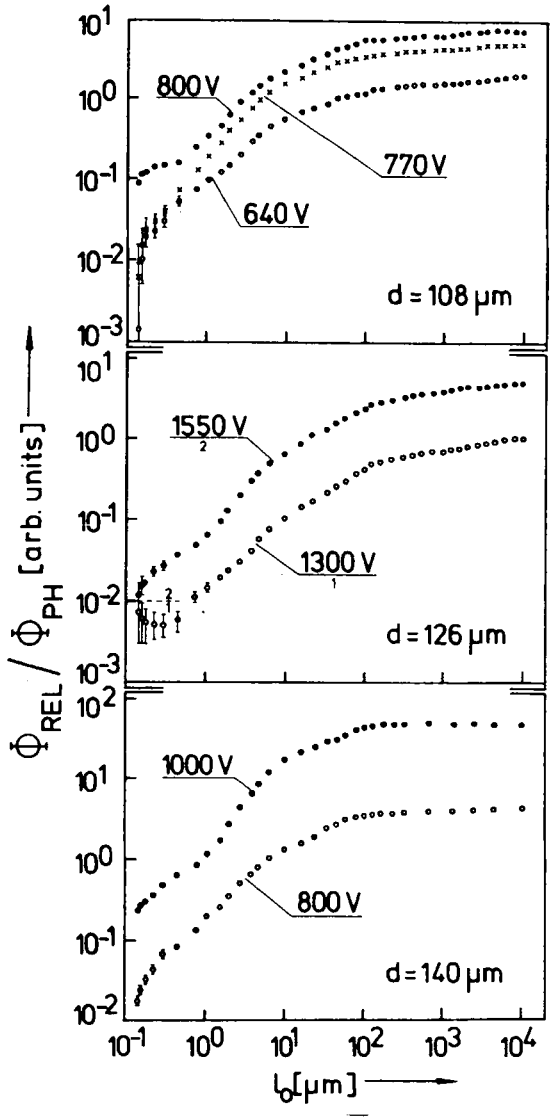

FIGURE 2(b) Experimental dependence of the recombination electroluminescence (Φ_{REL}) to photoluminescence (Φ_{PH}) ratio as a function of observation depth (l_0) for 5 different tetracene crystals with various voltages applied to the crystals when the REL was under measurements.

In contrast, within the short-wavelength ($l_0 \gtrsim 10^3$ μm), the observed change in the ratio Φ_{REL}/Φ_{PH} must be ascribed to a difference in the spatial distribution of emitting species, and this region gives essential informations on $\varphi(x)$.

The spatial distribution $\varphi(x)$ obtained on the basis of the experimental values of $F(l_0) = \Phi_{REL}(l_0)/\Phi_{PH}(l_0)$ from Figure 2 and the STREG-procedure

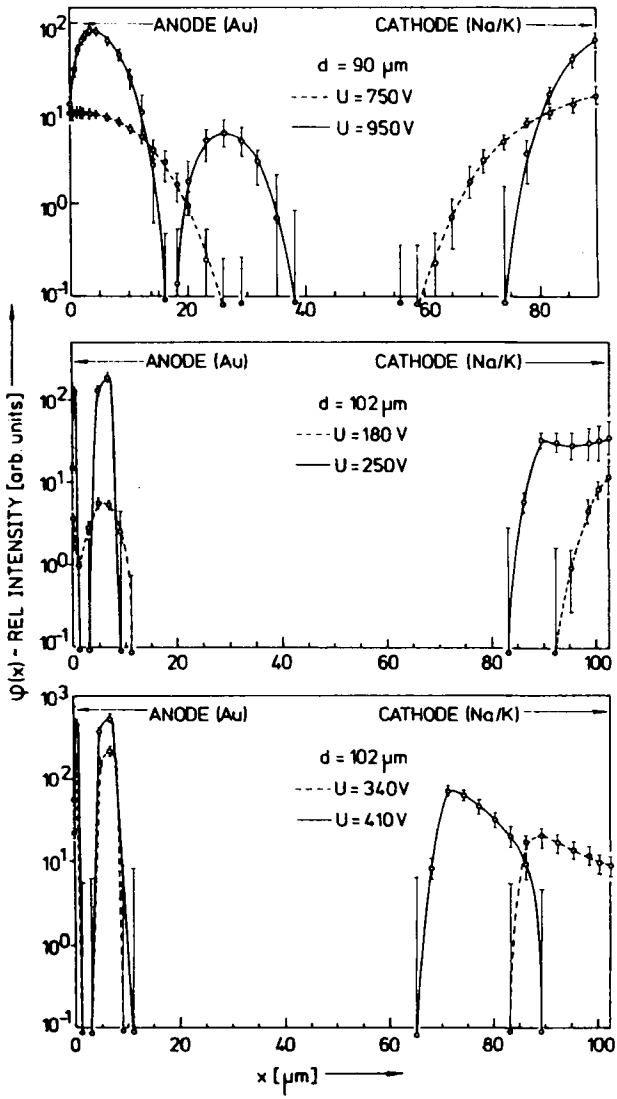

FIGURE 3(a) Spatial distribution of the electroluminescence in 5 tetracene single crystals at different voltages, obtained from the data of Figure 2 applying the STREG-procedure.

from Section 2, for 5 different crystals and various voltages, is shown in Figure 3.

The absence of an exact saturation of the ratio Φ_{REL}/Φ_{PH} for $10^3 \leq l_0 \leq 10^4$ μm, does not influence, significantly, the final form of the REL-distribution (see Figure 4).

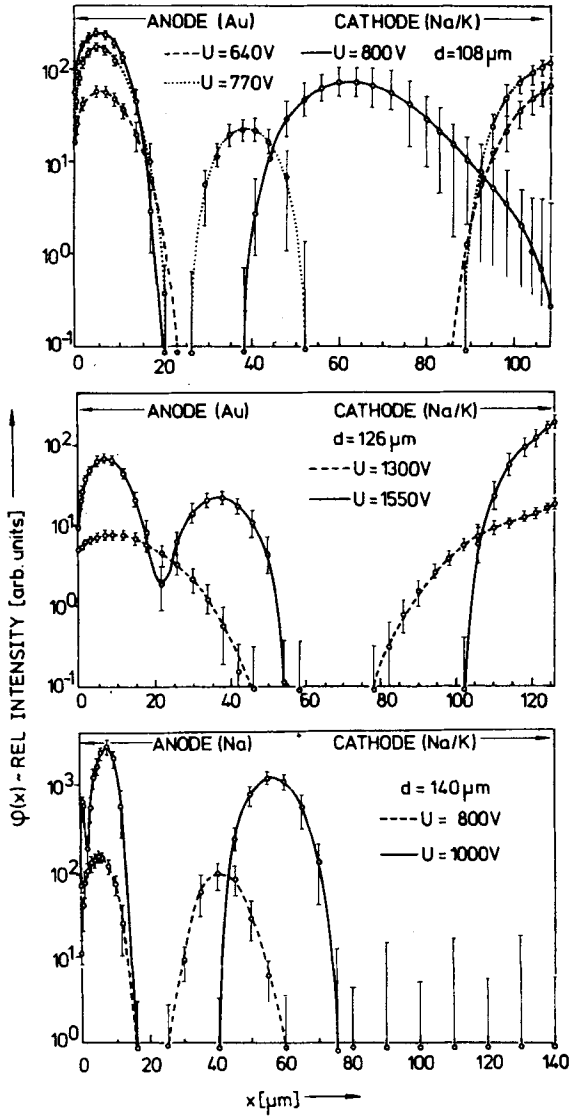

FIGURE 3(b) Spatial distribution of the electroluminescence in 5 tetracene single crystals at different voltages, obtained from the data of Figure 2 applying the STREG-procedure.

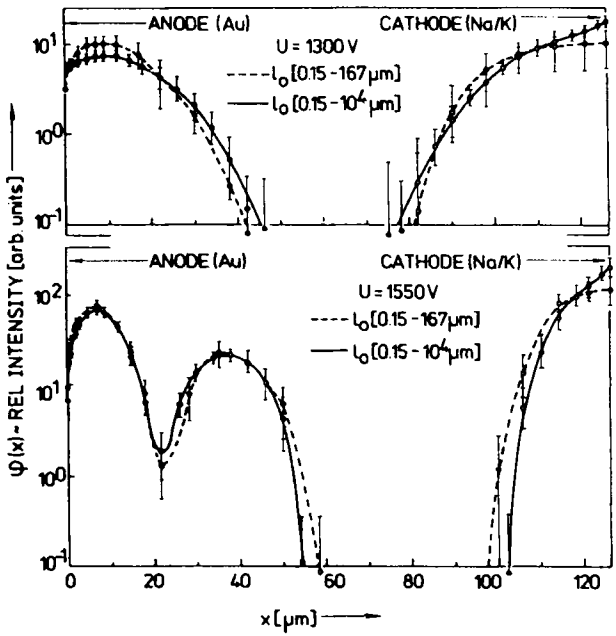

FIGURE 4 Illustration of maximal deviation in the spatial distribution of REL due to the difference between reabsorption free REL and PH emission spectra within the long wavelength region of a 126 μm-thick tetracene single crystal. The curves were obtained using the data from Figure 2 in two different ranges of l_0 (given in the square brackets). The crystal chosen shows maximal contribution of the trapped-exciton emission in the REL. This is seen as a continuous increase of Φ_{REL}/Φ_{PH} with increasing l_0 above the value $\sim 10^3$ μm (see Figure 2).

4 DISCUSSION

4.1 Relation to uni-polar-injection I–V characteristics

Tetracene is a typical organic molecular crystal, and due to its low fluorescence efficiency the approximation made to the method described in Section 2 could safely be utilized in determination of the spatial distribution of the REL.

In tetracene the mobilities of both carriers are of the same order of magnitude and one can use an average mobility along the c'-direction $\bar{\mu}_{c'} \cong 0.5\ \mathrm{cm^2/V \cdot s}$.[19]

This is comparable to the recombination mobility $\mu_0 \cong 1\ \mathrm{cm^2/V \cdot s}$ obtained with $\varepsilon = 4$ and $c = (1.0 \pm 0.5)\ 10^{-6}\ \mathrm{cm^3\ s^{-1}}$.[19]

In the absence of traps or in the shallow-trap case, this would correspond to VCC with the undivided recombination zone $L_R < d$. The results presented

in Figure 3 show that in all crystals used the recombination zone is split up at least in two layers.

This means that, in general, VCC in these crystals are limited by deep electron and hole traps what is confirmed by unipolar injection log I-log V plots shown in Figure 5.

It is interesting to note that the hole current in a given crystal was always considerably less than the electron current. The curves for hole injection show that traps exponential in energy are dominant for all of the crystals.

In some crystals, however, the curve for electron injection is typical for a single deep electron trap (see e.g. Figure 5a). The spatial distribution of the REL corresponding to such differences in energy distributions of traps for holes and for electrons may exhibit a luminous region placed somewhere

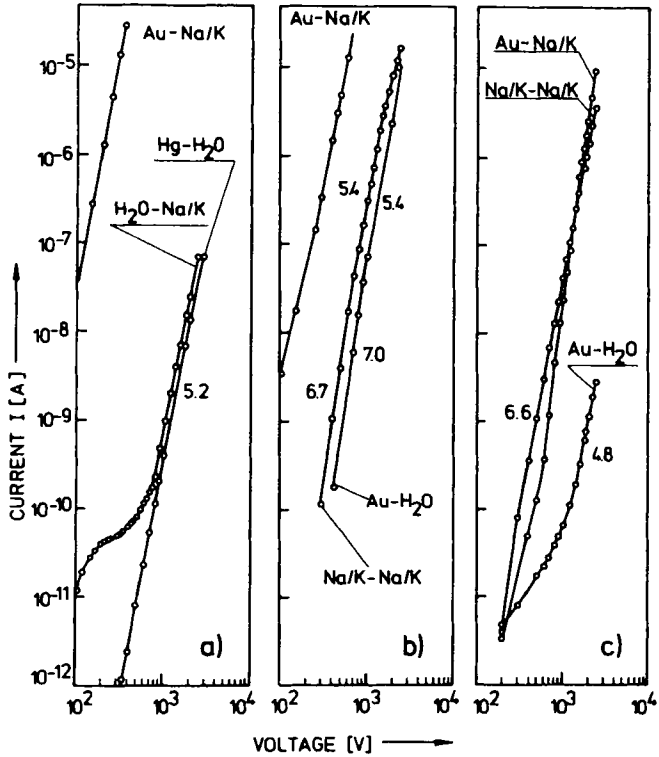

FIGURE 5 Current-voltage (I-V) relationships for chosen tetracene crystals provided with one or two injecting contacts described in the figure. The first symbol in all descriptions stands for the anode. The numbers at the uni-polar characteristics denote their log I-log V slopes. Part a: for uni-polar characteristics the thickness of the crystal $d = 233$ μm, for double injection $d = 102$ μm obtained by cutting from the first one; Part b: $d = 108$ μm; Part c: $d = 126$ μm.

The uni-polar characteristics were obtained with an additional measuring cell making possible replacement of the contacts to a given crystal.

between the anode luminous zone and the cathode. It has a more or less sharp boundary with the cathode dark space, depending on depth of the traps as well as on the voltage applied to the crystal.

The I–V dependences for a 108 μm-thick crystal (Figure 5b) show that below $\sim 10^3$ V, where the spatial distributions of the REL have been determined (see Figure 3), the characteristic trap parameter kT_c for holes is greater than that for electrons. This difference is seen much better for a 102 μm-thick crystal below ~ 800 V, where electron injection is typical for a single deep electron trap (Figure 5a).

Although, in both cases a luminous region separated from the cathode appears in the crystal at sufficiently high voltages, its shape and separation distance from the cathode is different (see Figure 3). The relative darkness of the cathode dark space is much more pronounced in the second of the two crystals considered. This could indicate that for electrons the thermal release time τ_{REL} and the trapping time τ_t are much longer than the recombination time τ_{REC}.

The recombination zone which is then confined to the double injection region,[5] but not identical with it makes the problem extremely difficult to deal with. Independent of voltage, no cathode-separated luminous zone could be found when kT_c for holes was smaller than that for electrons. This is the case illustrated in Figure 3 and Figure 5c.

These results indicate electron trapping levels to be deep and populated enough that similarly to the anode side, to make the recombination time (τ_{REC}) longer as compared to the trapping time (τ_t).

4.2 Splitting in the anode region

In contrast to the cathode region of the REL, at a sufficiently high voltage applied, a splitting up of the light emission zone in two layers appears in front of the anode (Figure 3).

Let us first consider a model of the effect based upon the following assumptions.

Let the experimental spatial distribution of the REL give directly the total recombination rate

$$r(x) = \frac{c}{e} n_f(x) p_t(x) \tag{5}$$

which according to continuity equation can be expressed by electron current density

$$j_n(x) = e\mu_n F(x) n_f(x) \tag{6}$$

as follows

$$\frac{dj_n(x)}{dx} = er(x). \tag{7}$$

Let the concentration of trapped holes $p_t(x)$ be much larger than the concentration $p_f(x)$ of free holes, $n_t(x)$-trapped and $n_f(x)$-free electrons.

Then, Poisson's equation can be approximated by

$$\varepsilon\varepsilon_0 \frac{dF(x)}{dx} = ep_t(x), \tag{8}$$

where $F(x)$ is the electric field strength, e the electronic charge, ε the permittivity of the crystal, ε_0 the permittivity of free space. μ_n in (6) denotes the electron mobility.

Note the assumption that the major recombination mechanism in the region is the recombination of free electrons with trapped holes.

The numerical solutions of the equation system (5) to (8) are graphically illustrated in Figure 6. The minimum at $x \cong 27$ μm in the $p_t(x)$-plot cannot

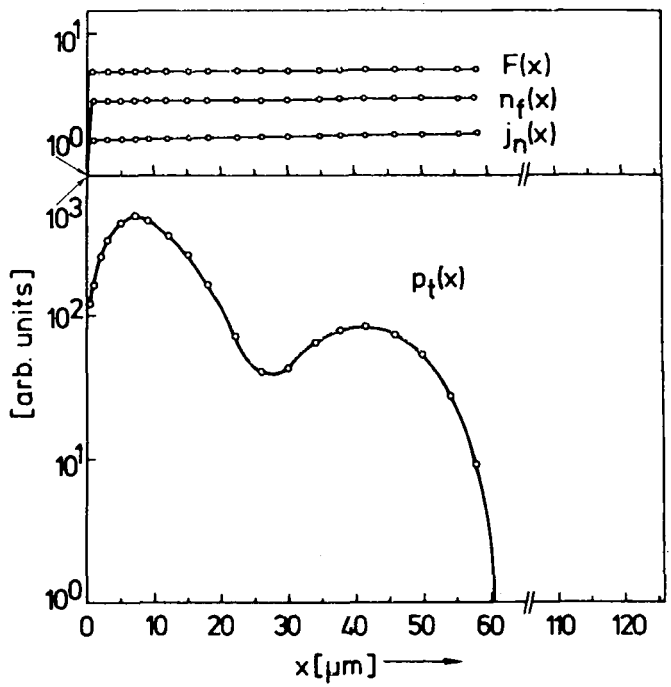

FIGURE 6 Calculated coordinate dependence of the trapped hole ($p_t(x)$) and free electron ($n_f(x)$) concentrations, the electric field $F(x)$ and the electron current density $j_n(x)$, obtained from Eqs. (5) to (8) with the assumption $\varphi(x) \equiv r(x)$.

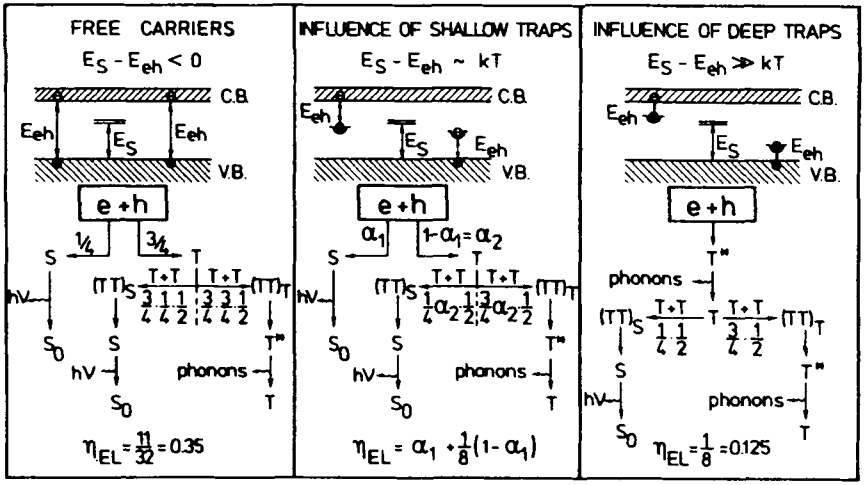

FIGURE 7 Simplified decay scheme of the excitation produced by recombination of an electron-hole pair. This scheme yields maximum values for the quantum efficiency (η_{EL}) under various trapping conditions. In order to get a real value of the quantum efficiency η_{EL} must be multiplied by the probability of radiative transition from the excited singlet state (S) into the ground state (S_0).

physically be rationalized and the euqlity $r(x) \equiv \varphi(x)$ must be questioned as it contains the assumption that the singlet exciton concentration follows exactly the total recombination rate.

In fact, due to spin statistics, three times more triplets than singlets are generated by free electron-free hole recombination (see Figure 7). The generated triplet excitons add to the triplet population produced in the very efficient process of the singlet exciton fission into two triplets at room temperature.[20]

The triplet excitons, in turn undergo the mutual annihilation leading to singlet excitons emitting photons of the DREL. The DREL emitted has time characteristic of $\sim 10^{-5}$ s.[10] Owing to the relatively efficient quenching of triplet excitons by trapped charge carriers,[21,22] the maximum concentration of the singlet excitons created in the bimolecular triplet annihilation is expected to occur farther from the anode as compared to the singlets emitting PREL.

A reconstruction of these two singlet exciton distributions is shown in Figure 8.

In the absence of space charge, the singlet and triplet exciton distributions are identical. A spatially inhomogeneous distribution of high density trapped holes ($p_t(x)$) in the region causes the triplets to be quenched much more efficient in the direction of the increasing charge density.

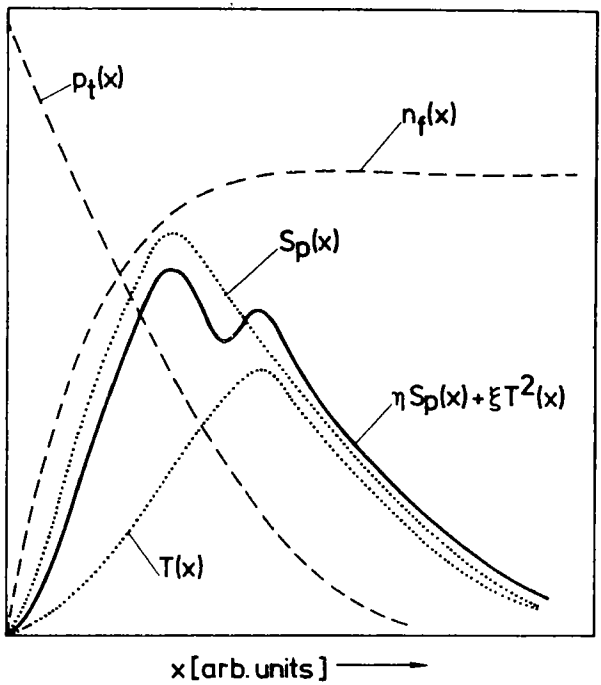

FIGURE 8 A schematic construction of the spatial distribution of the REL ($\eta S_p(x) + \xi T^2(x)$; η, ξ the coefficients transmitting the exciton populations into the light observed) based on spatial variations of $p_t(x)$, $n_f(x)$, $S_p(x)$ and $T(x)$. $S_p(x)$ stands for the concentration of singlet excitons produced directly from electron-hole recombination events; $T(x)$ is the triplet concentration involving triplet excitons quenching by the trapped charge $p_t(x)$.

As a result the position of the maximum concentration of the two-triplet-created singlet excitons will shift towards the bulk of the crystal.

Thus, two maxima of the REL should appear in correspondence to these two PREL- and DREL-responsible maxima of singlet concentrations, respectively.

To proceed the analysis initiated with the system of equations (5) to (8) we have to add equations describing the steady state density of singlets.

These, for a given x, can be written as follows

$$\frac{dS(x)}{dt} = \alpha_1 c p_t(x) n_f(x) - k_S S(x) + \tfrac{1}{2} f \gamma_{TT} T^2(x) = 0, \tag{9}$$

$$\frac{dT(x)}{dt} = (1 - \alpha_1) c p_t(x) n_f(x) + 2k_S S(x) - \beta T(x) - \tfrac{1}{2}(1 + f)\gamma_{TT} T^2(x) - \gamma_{Th} p_t(x) T(x) = 0. \tag{10}$$

Here α_1 is the probability of a recombining electron-hole pair to yield a singlet exciton, k_S is the rate constant for singlet exciton fission, γ_{TT} is the rate constant for triplet exciton fusion, f is the fraction of triplet annihilation events which lead to a singlet exciton, β is the reciprocal of the triplet exciton lifetime, and γ_{Th} is the rate constant for the annihilation of triplet excitons by trapped holes.

It follows from (9) and (10) that

$$S(x) = k_S^{-1}\{\alpha_1 c p_t(x) n_f(x) + \tfrac{1}{2} f(1-f)^{-2}\gamma_{TT}^{-1} \times [((\beta + \gamma_{Th} p_t(x))^2 + 2(1-f)(1+\alpha_1)\gamma_{TT} c p_t(x) n_f(x))^{1/2} - (\beta + \gamma_{Th} p_t(x))]^2\}. \quad (11)$$

Now, $S(x)$ can be identified with the experimentally determined spatial distribution of REL ($\varphi(x)$) and together with (5) to (8) gives the system of equations describing the charge and electrical field behaviour in the anode region.

In order to qualitatively check the model, we have arbitrarily assumed a monotonically decreasing function for $p_t(x)$ and a monotonically increasing function $n_f(x)$ (see Figure 9).

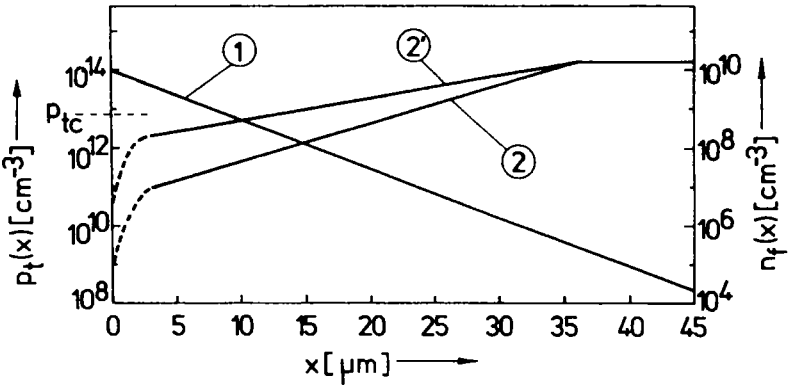

FIGURE 9 Spatial variations of $p_t(x)$ and $n_f(x)$ to be used in the construction of the function $\varphi(x)$ (see Figure 10). Note that $p_t(0) > p_{tc}$.

With these assumptions and $\alpha_1 = \frac{1}{4}$ (see Figure 7), on the basis of (5) to (8) and (11), we calculated $S(x)$. The result is shown in Figure 10.

We first calculated $S(x)$-distribution assuming only the prompt emission to be present in the crystal (Figure 10a). The curve reveals one maximum as must be expected for a product of monotonic functions $p_t(x)$ and $n_f(x)$ determining the singlet exciton concentration responsible for the PREL, $S(x) = k_S^{-1}\alpha_1 c p_t(x) n_f(x)$.

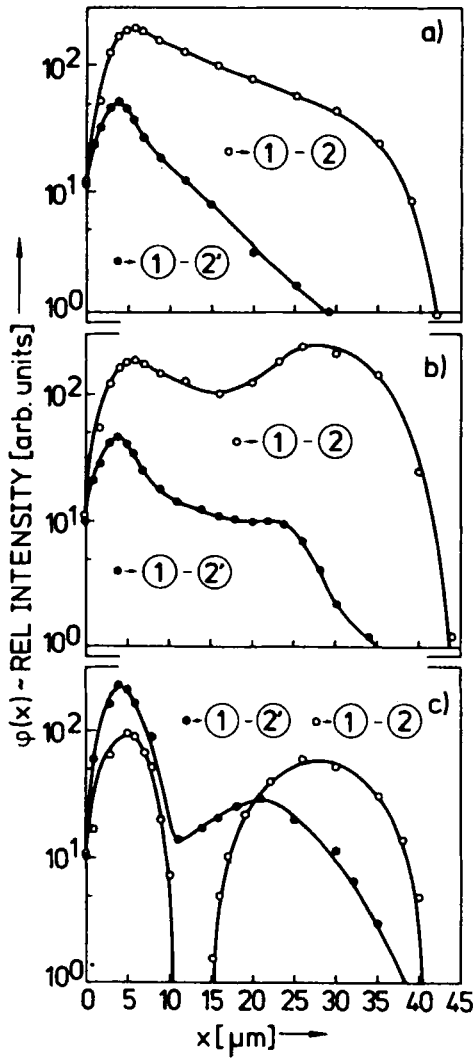

FIGURE 10 Variation of the REL intensity with position within the anode region for the problem of double injection into a real crystal with deep traps.

a) the curves obtained in the PREL-limit with $S(x) = k_S^{-1}\alpha_1 c p_t(x) n_f(x)$ and $\alpha_1 = \frac{1}{4}$;

b) the result involving the DREL quenched by the trapped charge (see Eq. 11) but still $\alpha_1(x) = \text{const} = \frac{1}{4}$;

c) the distributions modified by the $\alpha_1(x)$-function given by Eq. (15). The well-separated maxima appear when the appropriate gradient densities of $p_t(x)$ and $n_f(x)$ are taken from Figure 9.

The $S(x)$-dependence, according to the complete expression (11), neither for rapidly nor for slowly increasing function $n_f(x)$ can fit the experimental pattern of the two well-separated REL maxima† (Figure 10b, compare Figure 3). This could be caused by a relatively small contribution of the DREL to the total recombination radiation, resulted from the high value of α_1. Indeed, the used mean value of $\alpha_1 = \frac{1}{4}$ is valid for the electron-hole pair energy (E_{eh}), greater than the singlet exciton energy (E_S). This is, certainly, the case for free carriers (see Figure 7) but not for the recombination of free carriers with the carriers in traps for which $E_{eh} < E_S$ (see Figure 6b, c). In this case

$$\alpha_1 = \tfrac{1}{4} \exp\left[- \frac{E_S - E_{eh}}{kT} \right]. \tag{12}$$

It is, easily, seen that $\alpha_1 < \frac{1}{4}$ and in the limiting situation $E_{eh} \ll E_S$, $\alpha_1 \to 0$ so that the total electroluminescence efficiency comes to its minimum value $\eta_{EL} \cong 0.125$ (Figure 7).

If an exponential trap distribution rather than a single trapping level is present in a crystal the highest trap level occupied is approximated by the quasi-Fermi level $E_F(x)$ which, on the other hand, depends on the magnitude of the stored charge and hence on the applied voltage V. In such a case

$$\alpha_1 = \tfrac{1}{4} \exp\left\{ - \frac{E_F(x) - E_D}{kT} \right\}, \tag{13}$$

where E_D is the demarcation energy defined by $(E_g - E_S)$ with E_g standing for the energy gap. The density of trapped holes is then given by[1]

$$p_t(x) = H \exp\left[- \frac{E_F(x)}{kT_c} \right] \tag{14}$$

with H denoting the total concentration of hole traps. Hence, α_1 as a function of $p_t(x)$ can be obtained

$$\alpha_1(x) = \frac{1}{4} \left[\frac{p_t(x)}{H} \right]^t \exp\left(\frac{E_D}{kT} \right), \tag{15}$$

† Note that an increase in the slope of the function $n_f(x)$ is equivalent to a decrease in the slope of $p_t(x)$-distribution. Thus, one of the functions can be modified instead of changing both of them.

In principle, one can formally find a function $n_f(x)$ which combined with $p_t(x)$ would give $S(x)$ with two separated maxima. Such a function, however, has no physical reasoning as it should have a step-like shape.

where $l = T_c/T$ is to be determined from suitable slopes of the (log I–log V)-plots shown in Figure 4. Substituting $\alpha_1 = \frac{1}{4}$ yields the critical value of p_t,

$$p_{tc} = H \exp\left(-\frac{E_D}{lkT}\right) \tag{16}$$

such that for $p_t(x) \geq p_{tc}$ the probability α_1 will solely be determined by spin statistics.

Inserting Eq. (15) into expression (11) we obtain the concentration of singlet excitons modified by the x-dependence of α_1. As it is seen from Figure 10c a splitting up of $S(x) \sim \varphi(x)$ occurs for the $p_t(x)$ and $n_f(x)$ distributions used previously for checking $S(x)$ with $\alpha_1 = \frac{1}{4}$ (see Figure 9).

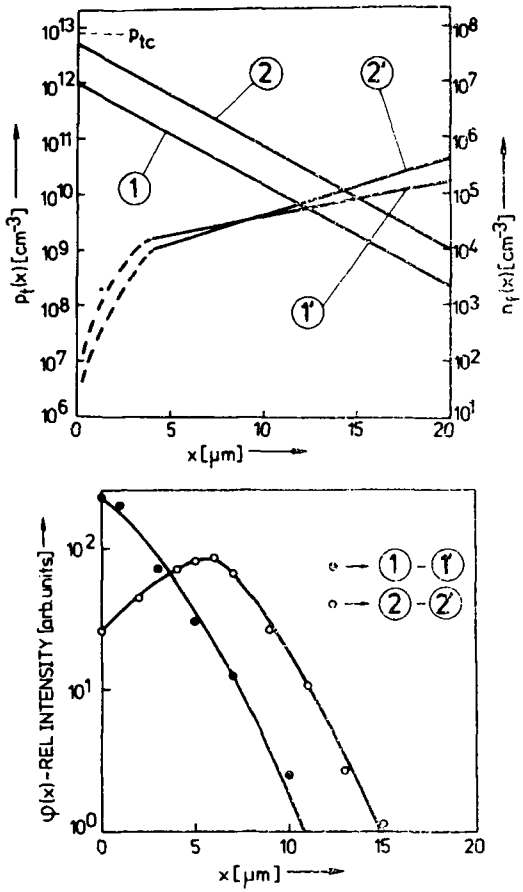

FIGURE 11 Theoretical REL distributions for $p_t(0) < p_{tc}$. A suitable combination of $p_t(x)$ and $n_f(x)$ gradients leads to different shapes of $\varphi(x)$ corresponding to various experimental cases demonstrated in Figure 3.

We note that the log-log plot of the $p_t - x$ distribution starts, in this case, from a value above $p_{tc} \cong 10^{13}$ cm^{-3}. This makes possible that for $x \lesssim 10$ μm singlet excitons are directly created with the relatively high ($\alpha_1 = \frac{1}{4}$) constant efficiency, so that the maximum placed closer to the anode can be attributed to the PREL.

The position of the second maximum ($x \cong 27$ μm) falls into the region where $p_t(x) < p_{tc}$ and α_1 is very small leading to production of a large concentration of triplet excitons. Consequently, this maximum is to be associated with the DREL.

Only one maximum belonging to the DREL should occur when $p_t(x)$ will start below p_{tc}.† This is the case illustrated in Figure 11. A suitable combination of $p_t(x)$ and $n_f(x)$ gradients permits the maximum to be properly shaped.

The two examples of Figure 11 correspond to the real situations shown in Figure 3 for lower voltages.

Finally, the model presented—based on the charge quenching of the delayed component of the REL and on the charge density-modification of the probability of a recombination electron-hole pair to yield a singlet exciton, gives a qualitative explanation of all our observations.

The experimentally obtained spatial REL-distributions, in turn, can be utilized for determination of the coordinate dependence of the carrier and current densities and of the electric field strength under double injection. This gives a new tool for checking different theories of VCC which still require refining of their choice of the relevant boundary conditions, and their treatment of carrier trapping.

Appendix A

Equation (3) is the linear Fredholm equation of the first kind, defined by

$$\int_a^b K(x, y)\varphi(x)dx = f(y), \qquad c \leq y \leq d, \tag{A.1}$$

where the kernel $K(x, y)$ and the right hand side $f(y)$ are given. This presents a classic example of an "ill-posed" problem, by which one means that the solution $\varphi(x)$ does not depend continuously on the data function $f(y)$. We must insist on the fact that in our case $f(y)$ is known only for $y \in \{y_j\}$

† It is worthy to note that the value of p_{tc} varies from crystal to crystal as p_{tc} is a function of trap parameter l (see Eq. 16).

($j = 1, 2, \ldots, m$) and that these data are given with known errors. With these inadequate data, to solve Eq. (A.1) is extremely difficult, in general.[23]

We solved Eq. (A.1) by the method of statistical regularization. It is one of the methods of regularization which proceed by converting an ill-posed problem into a well-posed one. This probabilistic method gives the best solution of our Eq. (3). We give here only a brief description of the main principles of the method for convenience referred to as the STREG method. More detailed information can be found in Ref. 14.

We can replace Eq. (A.1) by the set of finite-difference equations

$$\sum_{i=1}^{n} A_i K_{ji} \varphi_i + \delta_j = f_j, \qquad j = 1, 2, \ldots, m, \tag{A.2}$$

where A_i are the weights appropriate to the quadrature formula used to approximate the integral and f_i, φ_i, δ_j and K_{ji} are defined as $f_j = f(y_j)$, $\varphi_i = \varphi(x_i)$, $K_{ji} = K(x_i, y_j)$, δ_j-error of f_j.

In recognition of the fact that an actual experiment involves both sampling of $\boldsymbol{\varphi}$ and random errors of observations in $\mathbf{f}$, the function $\boldsymbol{\varphi}$ and $\mathbf{f}$ are now treated as a stationary random processes. Then, if we define the conditional probability† $P(\mathbf{f}|\boldsymbol{\varphi})$ and the probability $P(\boldsymbol{\varphi})$, we can use the apparatus of mathematical statistics known as the Bayesian strategy based on the Bayes' rule (e.g. Ref. 15)

$$P(\boldsymbol{\varphi}|\mathbf{f}) = \frac{P(\boldsymbol{\varphi})P(\mathbf{f}|\boldsymbol{\varphi})}{\int P(\boldsymbol{\varphi})P(\mathbf{f}|\boldsymbol{\varphi})d\varphi}, \tag{A.3}$$

so we can find the solution of Eq. (A.1).

Assuming that the errors are independent and normally distributed with the expectation equal to zero, $P(\mathbf{f}|\boldsymbol{\varphi})$ can be written as

$$P(\mathbf{f}|\boldsymbol{\varphi}) = \prod_{j=1}^{m} (2\pi s_j)^{-1/2} \exp\left\{ -\frac{1}{2s_j^2} \left[f_j - \sum_{i=1}^{n} K_{ji} \varphi_i \right]^2 \right\} \tag{A.4}$$

or, in more useful form, as

$$P(\mathbf{f}|\boldsymbol{\varphi}) = (2\pi s^2)^{-m/2} \exp\left\{ -\frac{1}{2s^2} |\mathbf{g} - L\boldsymbol{\varphi}|^2 \right\}, \tag{A.5}$$

where

$$s_j - \text{rms error of } f_j, \quad g_j = \frac{s}{s_j} f_j, \quad L_{ji} = \frac{s}{s_j} K_{ji}, \quad s^m = \prod_{j=1}^{m} s_j.$$

† For convenience the term "density of probability" is in whole section replaced by a simple "probability."

Now, to determine $P(\varphi)$ we need to introduce an a priori information about φ itself. In our case it is an information about the smoothness of the solution. The assumption of the smoothness of the unknown function is done in the STREG method by imposing the probabilistic restriction on the value of a certain functional being the finite-difference approximation of Euclidean norm of the second derivative

$$\Omega[\varphi(x)] = \int \left[\frac{d^2\varphi(x)}{dx^2}\right]^2 dx. \tag{A.6}$$

Then, it can be shown that the probability $P(\varphi)$ has the following form:

$$P_\alpha(\varphi) = C_\alpha \exp\left\{-\frac{\alpha}{2}(\varphi, \Omega\varphi)\right\}, \tag{A.7}$$

where $\alpha > 0$ is a parameter characterizing the smoothness of the unknown function. C_α is the normalizing coefficient dependent on α.

The average value of the functional $\Omega(\varphi)$ over this probability is n/α. The functions φ for which $\Omega(\varphi)$ is noticeably greater than n/α are suppressed by the exponent in $P_\alpha(\varphi)$. If the approximate value of the functional $\Omega(\varphi)$ is known, we can estimate α and take $P_\alpha(\varphi)$ as an a priori probability for φ. Now, applying the Bayesian strategy, we can obtain a regularized solution and its rms error from the equations

$$(L^*L + s^2\alpha\Omega)\varphi_\alpha = L^*\mathbf{g}, \tag{A.8}$$

$$\sigma_i^2 = s^2[(L^*L + s^2\alpha\Omega)^{-1}]_{ii}, \tag{A.9}$$

where σ_i-rms error of φ_i.

The above presented version of the STREG method requires an a priori information on parameter α, i.e. an a priori estimate of the value of the $\Omega(\varphi)$ functional. In our case, this information is not available and a more complicated variant of the method is used. We can find α as an a posteriori estimate from the experimental data by analysing the conditional probability $P(\alpha|\mathbf{f})$ which has the form

$$P(\alpha|\mathbf{f}) = \frac{P(\alpha)\int P(\mathbf{f}|\varphi)P_\alpha(\varphi)d\varphi}{\iint P(\alpha)P(\mathbf{f}|\varphi)P_\alpha(\varphi)d\varphi d\alpha}. \tag{A.10}$$

When the experiment is sufficiently informative (usually it is enough that $n > 10$), the probability $P(\alpha|\mathbf{f})$ has a sharp maximum for some $\alpha = \alpha_0$. Therefore, we can calculate α_0 from (A.10) in the usual way, from its first derivative, and obtain a solution from (A.8) and (A.9) by putting $\alpha = \alpha_0$.

Appendix B

The computer program for STREG method is complicated and before the analysis of our experimental data we tested it in two ways.

i) We assumed an unknown function $\varphi(x)$. We put it into Eq. (3) and after an integration for different l_0 we get $f_j(l_0)$—the right hand side of Eq. (3). Then, we assumed the magnitude of rms errors s_j for calculated $f_j(l_0)$ and we put $f_j(l_0)$ and s_j as entry data in STREG program. For simple geometrical tests such as e^{-x}, a^x, x^2, x^{-1} the error of restoration was less then 0.1%. The worst result of one of more complicated tests is shown in Figure 12. As

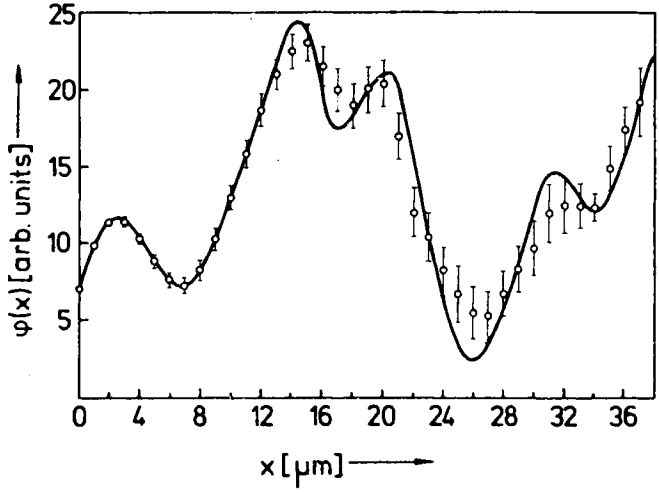

FIGURE 12 The STREG-restoration (circles) of an arbitrarily assumed function $\varphi(x)$ (solid line).

can be seen, the accuracy of reconstruction decreases with increasing x, but the restored function conserves the shape of the assumed one. This decrease of accuracy towards increasing x is mainly connected with fast decreasing of the exponential kernel in Eq. (3).

ii) We experimentally determined the steady-state singlet distribution in photoluminescence of tetracene crystals. If we replace the Eq. (1) by the equation of type 2 with $S(x)$ corresponding to another penetration depth of the exciting light, the STREG program gives the space distribution of photoluminescence in a crystal. The distribution should have an exponential shape and one of the results is shown in Figure 13.

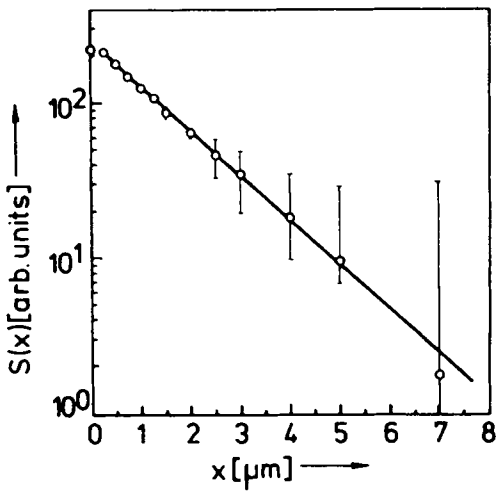

FIGURE 13 The STREG-determination of the steady-state singlet distribution in photoluminescence of a tetracene crystal, excited with the light of wavelength λ_a = 366 nm.

We have made several tests of both kind and all the tests proved that the STREG program is formally correct and that the results of our experiments are sufficiently informative to be treated by the method of statistical regularization.

References

1. W. Helfrich, in *Physics and Chemistry of the Organic Solid State*, Vol. III (D. Fox, M. M. Labes, and A. Weissberger, Eds.), John Wiley and Sons, Inc., 1967, p. 1.
2. M. A. Lampert and P. Mark, *Current Injection in Solids*, Academic Press, New York and London, 1970.
3. M. A. Lampert and R. B. Schilling, in *Semiconductors and Semimetals*, Vol. 6 (R. K. Willardson and A. C. Beer, Eds.), Academic Press, New York and London, 1970, p. 1.
4. H. P. Schwob and I. Zschokke-Gränacher, *Solid State Electron.*, **15**, 271 (1972).
5. H. P. Schwob and D. F. Williams, *J. Appl. Phys.*, **45**, 2638 (1974).
6. J. Dresner, *R.C.A. Review*, **30**, 322 (1968).
7. H. Baessler, G. Herrmann, N. Riehl, and G. Vaubel, *J. Phys. Chem. Solids*, **30**, 1579 (1969).
8. G. P. Owen, J. Sworakowski, J. M. Thomas, D. F. Williams, and J. O. Williams, *J. Chem. Soc. Faraday Trans. II*, **70**, 853 (1974).
9. J. Kalinowski and J. Godlewski, *Chem. Phys. Letters*, **36**, 345 (1975).
10. J. Kalinowski, J. Godlewski, and R. Signerski, *Mol. Cryst. Liq. Cryst.*, **33**, 247 (1976).
11. J. Kalinowski, J. Godlewski, and J. Gliński, *J. Luminescence*, in print.
12. A. W. Smith and C. Weiss, *Chem. Phys. Letters*, **14**, 507 (1972).
13. R. Alfano, S. Shapiro, and M. Pope, *Optics Commun.*, **9**, 388 (1973).
14. V. F. Turchin, V. P. Kozlov, and M. S. Malkevich, *Usp. Fiz. Nauk*, **102**, 345 (1970).
15. H. G. Tucker, *An Introduction to Probability and Mathematical Statistics*, Academic Press, New York, 1962.
16. A. Bree and L. E. Lyons, *J. Chem. Soc.*, 5206 (1960).
17. B. J. Mulder, Philips Res. Rpts. Supplement 4 (1968).

18. W. Arden, M. Kotani, and L. M. Peter, *Phys. Stat. Sol.* (b), **75**, 621 (1976).
19. P. Schlotter, J. Kalinowski and H. Baessler, *Phys. Stat. Sol.* (b), **81**, 521 (1977).
20. C. E. Swenberg and N. E. Geacintov, in *Organic Molecular Photophysics*, Vol. I (J. B. Birks, Ed.), Wiley, New York, 1973, ch. 10.
21. J. Kalinowski and J. Godlewski, *Phys. Stat. Sol.* (a), **20**, 403 (1973).
22. J. Kalinowski and J. Godlewski, *Chem. Phys.*, in print.
23. G. F. Miller, in *Numerical Solution of Integral Equations* (L. M. Delves and J. Walsh, Eds.), Oxford University Press, 1974, ch. 13.
24. G. Vaubel and H. Baessler, *Mol. Cryst. Liq. Cryst.*, **12**, 47 (1970).